Reliability Engineering and System Safety 203 (2020) 107085

Contents lists available at ScienceDirect

Reliability Engineering and System Safety

journal homepage: www.elsevier.com/locate/ress

Time-dependent reliability analysis of service-proven quay walls subject to corrosion-induced degradation

Alfred A. Roubos[a,*], Diego L. Allaix[b], Timo Schweckendiek[c], Raphael D.J.M. Steenbergen[d], Sebastiaan N. Jonkman[e]

[a] Department of Hydraulic Engineering, Port of Rotterdam, Port Development, TU Delft, Netherlands
[b] Department of Structural Engineering, TNO, Built Environment and Geosciences, Ghent University, Belgium
[c] Department of Hydraulic Engineering, Deltares, Geo/Engineering, TU Delft, Netherlands
[d] Department of Structural Engineering, TNO, Built Environment and Geosciences, Ghent University, Belgium
[e] Department of Hydraulic Engineering, TU Delft, Netherlands

ARTICLE INFO

Keywords:
Corrosion
Time-dependent reliability analysis
Reliability index
Service-proven quay wall

ABSTRACT

The assessment of service-proven quay walls subject to corrosion-induced degradation is inherently a time-dependent reliability problem. Two major challenges are the modelling of corrosion and taking into account the decrease of epistemic uncertainty throughout the quay wall's service life. The main objective of this study is to examine the probability of failure, despite successful past performance, when the quay wall is subject to corrosion and randomly imposed variable loads. The development of the annual failure rate is modelled using crude Monte Carlo and by performing a first-order system reliability analysis. The annual failure rates found for service-proven quay walls vary over time. For those with successful service histories and subject to low corrosion rates, the highest reliability indices are observed in the first year of the service life, whereas with higher corrosion rates the final year prevails. In general, it seems more practical to evaluate reliability on an annual basis rather than over longer time periods, since the latter will introduce an iterative procedure to determine the wall's remaining lifetime. The key findings of this study can be crucial for the lifetime extension of existing quay walls, and presumably also for other service-proven geotechnical structures subject to corrosion.

1. Introduction

Marine structures such as quay walls and jetties often suffer from corrosion-induced degradation. In the coming years, many such structures throughout the world will approach the end of their design lifetime and will be reassessed as part of lifetime-extension programmes [46]. Steel structural members of quay walls generally show some degree of wall-thickness loss after a certain exposure period. This decrease in strength needs to be taken into consideration in the reassessment of quay walls. Two recent studies [9,55] show that the uncertainty in material loss due to corrosion-induced degradation significantly influences the reliability level of soil-retaining walls.

The parameters that influence corrosion can generally be classified into endogenous parameters related to the steel material, exogenous parameters related to the environment and a time-dependent component related to the exposure period [17]. In the port of Rotterdam, corrosion rates depend mainly on geometry, orientation and the type of marine structure concerned, as well as site-specific environmental conditions [23,24]. The wide diversity of deterioration agents, such as dissolved oxygen, salinity, water quality, temperature and exposure period makes predicting the corrosion phenomenon a fairly complex process [36,37]. There tends to be a rather high level of uncertainty associated with the various influences [35,38,39].

Consequently, millions of wall-thickness measurements and multiple destructive coupon tests have been performed in order to study the impact of uniform and pitting corrosion in the port of Rotterdam [24]. On the basis of this information, the Port of Rotterdam Authority has developed a practical method (Section 2) to assess the effect of corrosion on the remaining 'factor of safety' (*FoS*) using field observations. It is unclear, however, if a constant and time-independent factor of safety adequately covers the actual reliability level of a quay wall that has successfully been in service for a certain period of time, since in the absence of degradation it has become more likely that this structure will remain satisfactory and safe [39].

Only a few studies have investigated the influence of corrosion on

* Corresponding author.
E-mail addresses: aa.roubos@portofrotterdam.com (A.A. Roubos), diego.allaix@tno.nl (D.L. Allaix), timo.schweckendiek@deltares.nl (T. Schweckendiek), raphael.steenbergen@tno.nl (R.D.J.M. Steenbergen), s.n.Jonkman@tudelft.nl (S.N. Jonkman).

https://doi.org/10.1016/j.ress.2020.107085
Received 1 March 2019; Received in revised form 12 February 2020; Accepted 18 June 2020
Available online 20 June 2020

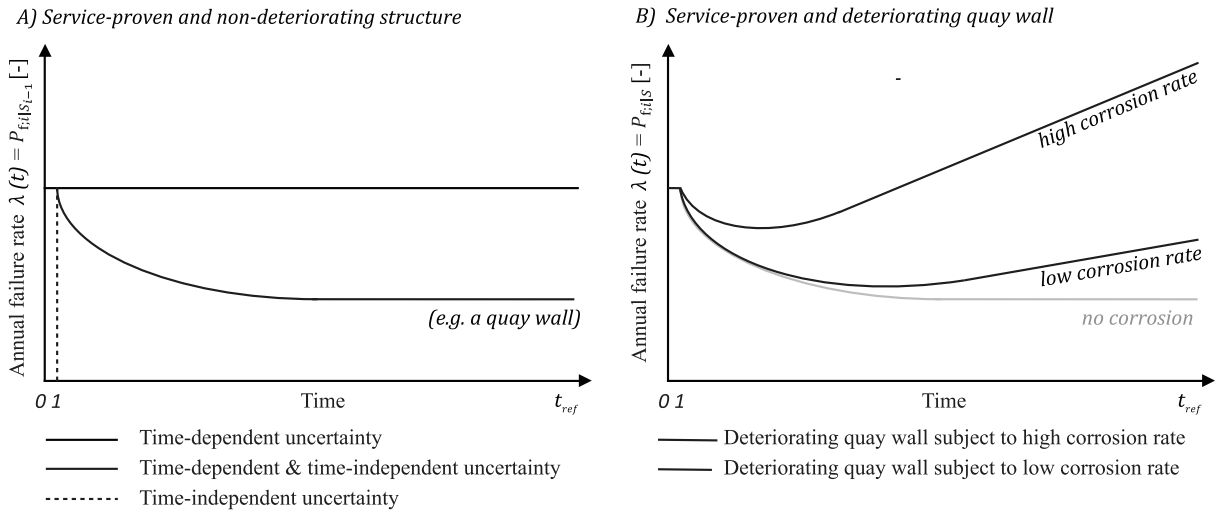

Fig. 1. Failure rate of service-proven, and non-deteriorating structures (A); and the effect of service-proven deteriorating quay walls (B).

the reliability of steel soil-retaining walls [17,40,51], mainly using the first-order reliability method (*FORM*). None of these studies took successful past performance into account, however, and so they most likely overestimate the probability of failure of service-proven soil-retaining walls. This is because not all effects of the passage of time and service on structural reliability are negative [14]. Hall [14] found that the failure rate of non-deteriorating structures with successful service histories decreases significantly over time if the initial uncertainty in time-independent random variables is high. Fig. 1A shows that a structure without degradation has a constant failure rate if all the uncertainty involved is variability in time, or in other words unlimited data will not reduce the inherent uncertainty in time [59]. By contrast, the failure rate of a structure will approach zero directly after completion if we assume that the uncertainty is exclusively epistemic in nature, since it only involves time-invariant random variables.

In reality, a quay wall will be subject to both time-dependent and time-independent sources of uncertainty, such as inherent natural variability in strength and loads (aleatory uncertainty), as well as lack of knowledge or insufficient information (epistemic uncertainty) [20]. In quay-wall engineering, time-independent uncertainties in soil properties [47] and model uncertainty significantly influence the reliability level [42]. It is therefore expected that the annual failure rate of a service-proven and non-deteriorating quay wall will decrease during its early years of service and over time approach a constant value, since after a period of successful service only the time-dependent (aleatory) uncertainty remains (Fig. 1A). If the effect of corrosion is included, the failure rate of the quay wall is expected to increase over time as the structure becomes subject to corrosion-induced degradation (Fig. 1B). The extent of this effect will depend on the corrosion rate. In addition, Fig. 1B shows that the beneficial effects of past performance can partly offset negative effects induced by corrosion.

The primary aim of this research is to analyse the effect of corrosion-induced degradation on the reliability of steel structural members of quay walls. A secondary aim is to show how the overall factor of safety (*FoS*) and the reliability index (β) are related, and how they change over time for systems subject to corrosion. When assessing the impact of wall-thickness loss on structural reliability, our particular interest was to determine the annual failure rate of service-proven quay walls. In this study, a time-dependent reliability analysis was performed by introducing time-independent and time-dependent uncertainty as random variables in order to account simultaneously for successful past performance and corrosion [4,48,50]. In addition, a sensitivity analysis reveals the impact of the variability in dominant parameters, such as soil strength, yield strength, live loads and corrosion, on the evolution of the reliability index over time. The results of this study have been used to reflect on the 'allowable stress-based' method, which is presently used to assess combi-walls subject to corrosion-induced degradation in Rotterdam (Section 2).

2. Allowable stress-based method to assess corroded combi-walls

This section describes the main principles of the 'allowable stress-based' method presently used by the Port of Rotterdam Authority to facilitate predictive asset management [58] by evaluating the structural integrity of steel combi-walls, which represent about half of the quay walls in its port. In the coming years, it is expected that the allowable stress-based method will be replaced by applying partial factors to load and resistance parameters. For more in-depth details, the reader is referred to the corrosion handbook by Jongbloed [24], which includes an overview of all research conducted into the phenomenon of corrosion at the port of Rotterdam.

A combined quay wall consists of steel primary elements such as H-profiles (Fig. 2A) or tubular piles (Fig. 2B), with sheet piles in between, which only have a soil retaining function. The corrosion rate of the primary steel element is usually higher due to a galvanic reaction with the secondary elements. This is because these elements generally have a higher steel quality, and hence are the less precious metal [21]. Furthermore, the wall-thickness loss on the landside of the primary elements appears to be negligible compared with the loss on the waterside, most likely because there is a lack of oxygen in the soil [24]. The wall-thickness reduction Δt is therefore only taken into account on the waterside of primary elements (Fig. 1).

The foundation for assessing corrosion-induced degradation relies on a strict in-situ test protocol using ultrasonic wall-thickness measurements and a procedure for measuring local corrosion pits [45]. Significant pitting not only affects the structural failure modes but can also introduce geometrical openings which may cause soil erosion directly behind the quay wall. The field observations are examined statistically in order to assess both these failure modes.

Over the years, the Port of Rotterdam Authority has collected a large number of wall-thickness measurements in salt, brackish and fresh-water conditions. Although the corrosion rates found align with those described in the literature, it appears that predicting corrosion without field observations is fairly difficult. Even quay walls with similar geometries and in similar environmental conditions may show significant differences in corrosion rates [24]. Clear correlations between corrosion and other deterioration agents have not yet been identified. Jongbloed interpreted all the information available and developed dedicated typical corrosion curves (Fig. 3B) for all the ports in the Netherlands [12]. If wall-thickness

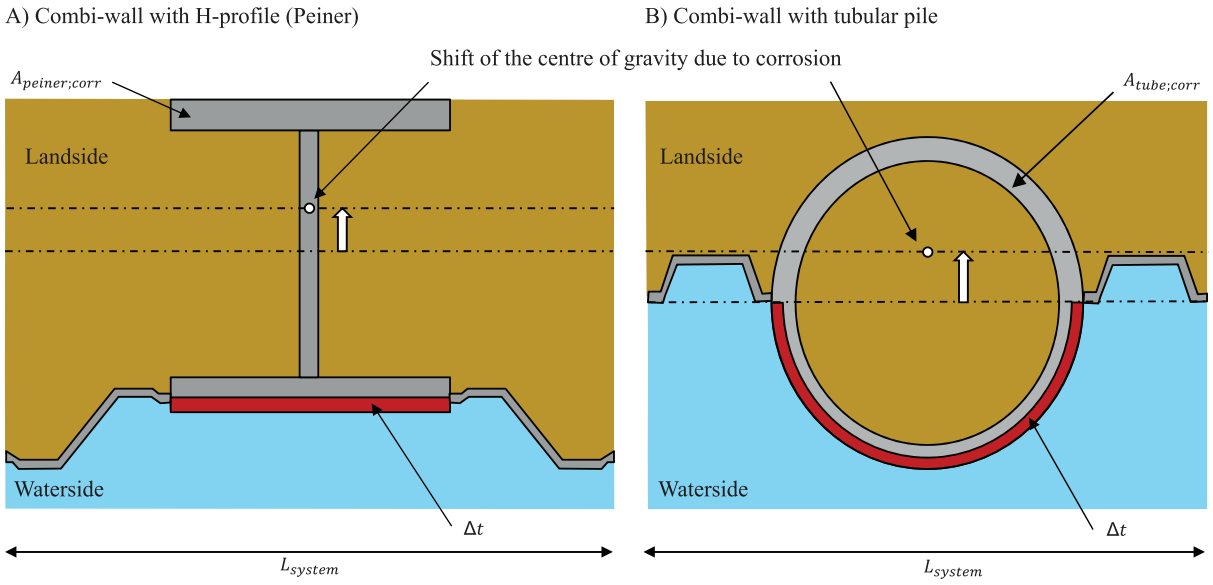

Fig. 2. Residual wall thickness and corrosion Δt of the primary combi-wall elements; cross-sections of Peiner system with H-piles (A) and of combi-tube system (B). The parts where corrosion is considered are highlighted in red. (For interpretation of the references to colour in this figure legend, the reader is referred to the web version of this article.)

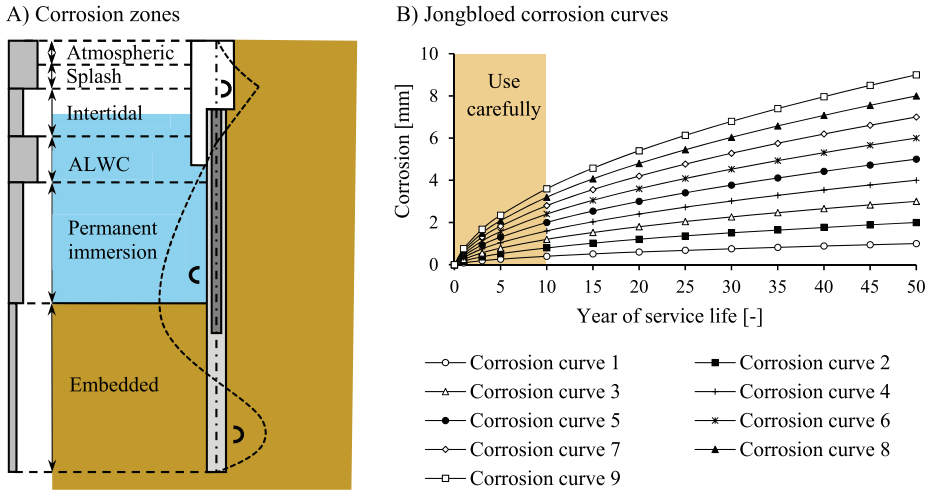

Fig. 3. Typical corrosion zones (A) and the Jongbloed corrosion curves (B).

measurements have been taken after a certain exposure period, the representative corrosion curve can be selected and extrapolated to predict the evolution of corrosion over time. It should be noted that Jongbloed's curves represent the equivalent mean value of corrosion Δt_{eq}, which equals the sum of the mean uniform and pitting corrosion with an accuracy of approximately 1 mm during an exposure period of 50 years [24]. When developing these curves, however, data from the first ten years was lacking and so the curves have only been verified for longer-term exposures.

The corrosion rates differ across the height of the quay wall, and therefore different corrosion zones are distinguished. These include the atmospheric, splash, intertidal, accelerated low-water corrosion (ALWC), permanent immersion and embedded zones (Fig. 3A).

Geometrical openings induced by pitting corrosion generally occur in the ALWC zone [12]. Since the corrosion rates of the secondary sheet piles are fairly low, soil erosion due to geometric openings is not very likely in case of combi-walls and has yet to be observed in reality. This is because a hole in a tubular pile does not result directly in a geometrical opening, whereas the flange thickness of H-piles is relatively large. At present, the remaining service life is generally determined by ascertaining when the yield stress in the outer fiber of structural members subject to corrosion becomes excessive. These stresses largely depend on bending moments and axial forces (Eq. (1)), and mostly prevail in the permanent immersion zone (Fig. 3A). In order to assess the influence of pitting corrosion [27], a geometrical reduction is applied to the initial wall thickness ($t_0 - \Delta t_{eq}$), resulting in the 'equivalent wall thickness' t_{eq} (Eq. (3)). It should be noted that Eq. (1) does not include the stress increase due to small bending moments introduced by eccentricity time normal force, since they are generally fairly low compared to the other components. This geometrical factor represents the decrease in the net capacity of the cross-section, and it depends on the ratio between pitting corrosion and residual wall thickness [24]. Although the structural assessment of corrosion relies on the *FoS* (Eq. (4)), the use of partial factors of safety is preferred.

$$\sigma_y(z, t_{eq}) = \frac{M_{wall}(z)}{W_{wall}(z, t_{eq})} + \frac{N_{tube}(z)}{A_{tube}(z, t_{eq})} \quad (1)$$

$$\sigma_{y;k;max}(z, t_{eq}) = \max(\sigma_{y;k}(z, t_{eq})) \quad (2)$$

$$t_{eq}(z) = t_0 - \Delta t_{eq}(z) \quad (3)$$

$$FoS = \frac{f_{y;k}}{\sigma_{y;k}} \quad (4)$$

Where:

t_{eq} Equivalent wall thickness for a particular corrosion zone [m]
t_0Initial wall thickness [m]
Δt_{eq} Equivalent wall-thickness loss due to uniform and pitting corrosion [m]
FoS Factor of safety [-]
$f_{y;k}$ Characteristic value yield strength [N/m^2]
σ_y Stress in outer fiber of tube [N/m^2]
$\sigma_{y;k}$ Stress in outer fiber of tube related to characteristic loads and material properties [N/m^2]
M_{wall} Bending moment in combi-wall [kNm/m^1]
N_{tube} Axial force at position of maximum bending moment in combi-wall [kNm/m^1]
$W_{combi\text{-}wall}$ Section modules of combi-wall [m^3/m^1]
A_{tube} Sectional area of tube [m^2/m^1]
z Depth [m]

Until the end of the twentieth century, the stresses σ_y were calculated using Blum's method [8]. Nowadays, however, finite element models are available to model the soil-structure interaction more accurately. When using Blum's method, it was common practice to apply a factor of safety to $\sigma_{y;k}$ to verify the nominal yield strength $f_{y;k}$. The minimum *FoS* required in the design of a new quay wall was 1.5. This does not remain constant, however: asset managers distinguish different stages (Fig. 4) in a quay wall's service life. As long as the *FoS* remains higher than 1.3, an existing quay wall is considered to be sufficiently safe; if the remaining *FoS* is between 1.2 and 1.3, the wall-thickness loss is monitored more frequently. An *FoS* lower than 1.2 is considered unacceptable, because then the quay wall may not be able to withstand 'accidental' any more, e.g. the accidental limit states will be exceeded. In the latter case, the quay wall must be retrofitted or replaced.

3. Reliability-based method to assess corrosion-induced degradation

3.1. Introduction

This section introduces the methods and input used to determine the effect of corrosion-induced degradation on the reliability of service-proven quay walls over time. In this study, a quay wall that has actually been built in Rotterdam serves as a reference (Fig. 5). This structure consists of a concrete slab and a combi-wall, and is equipped with grout anchors. The original design model and the as-built information were consulted [56]. Fig. 5 shows the associated diagrams of the bending moments, the normal force and the horizontal deformation in 'design' conditions, which represent the fundamental ultimate limit state (ULS). It should be noted that the highest stresses occur at the position of the maximum bending moment in the span, which is in the 'permanent immersion' zone (Fig. 5).

The failure modes affected by corrosion were reformulated on the basis of limit state functions (Section 3.2) using random variables (Section 3.3).

The assessment of service-proven structures is inherently a time-dependent reliability problem [14]. The main objective is to determine the probability of failure, after successful past performance, while the quay wall is subject to corrosion-induced degradation and randomly imposed variable loads. This problem was solved numerically by performing a crude Monte Carlo analysis (Section 3.4) for each year of service life, with Blum's method used to model the quay wall analytically [8]. It is well known that this method has some limitations, however, and so its calculation results were calibrated using a finite element model (Section 3.5).

3.2. Limit state functions of combi-walls subject to corrosion

Since structural failure modes generally determine the remaining service life of a combi-wall subject to corrosion (Section 2), this study focuses on the limit states for 'yielding' and 'buckling'. Fig. 5 shows that the stresses in outer fiber on the waterside $\sigma_{y;water}$ are generally lower than on the landside $\sigma_{y;land}$, due to the presence of the axial force N_{tube} (Fig. 6). As a result, the landside of the combi-wall is more susceptible to local buckling, whereas the development of the stresses on the waterside is more sensitive to corrosion. The wall-thickness loss on the waterside results in a proportional increase of $\sigma_{y;water}$ and a slight increase of $\sigma_{y;land}$ (Fig. 6). This is caused by a decrease of A_{tube}, a shift of the center of gravity and the reduction of the section modules on the waterside $W_{wall;water}$. Consequently, the effect of corrosion on the yielding capacity of the combi-wall was studied for both the landside (Eq. (5)) and the waterside (Eq. (6)).

The formula to evaluate local buckling (Eq. (7)) was derived from recent experiments, including the following empirical formula for the buckling factor f_B (Eq. (8)), which represents the ratio between the actual and the theoretical bending moment capacity [41]. The risk of local buckling is stress and strain level-dependent, and hence the parameter $D_{tube}/t_{tube}\varepsilon^2$ is generally used instead of D_{tube}/t_{tube}. The tubes' diameter *Dtube* and wall thickness *ttube* represent the dimensions, and the yield strength f_y was based on tensile tests. Particularly because f_B was determined from experiments (best fit), in this study we included an additional stochastic factor θ_B to account for model uncertainty. In addition, the model factors θ_M and θ_N were applied to the calculated bending

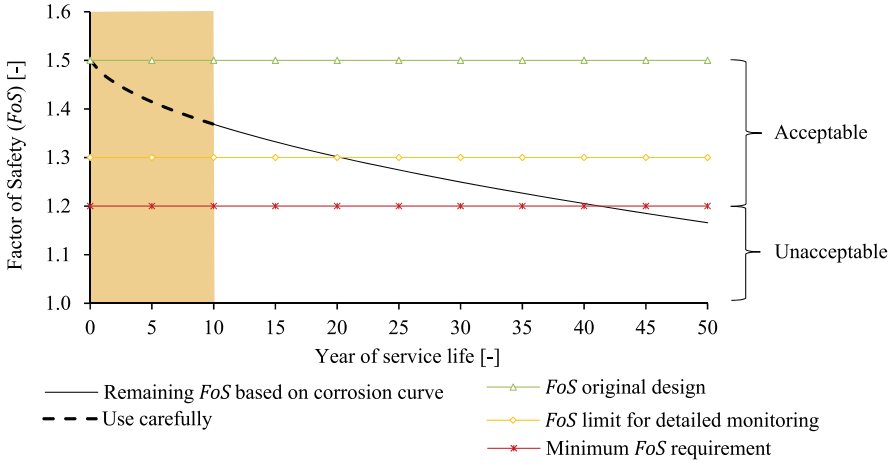

Fig. 4. Typical degradation curve due to corrosion and asset management stages of steel combi-tubes in Rotterdam.

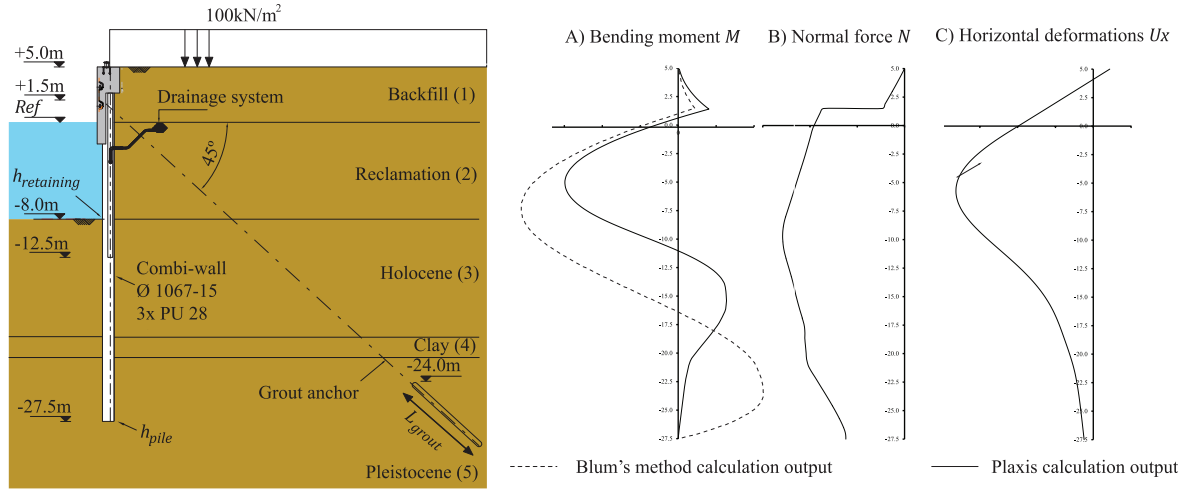

Fig. 5. Main dimensions of the reference quay wall, a combi-wall with grouted anchor (left), and its typical bending moment (A), normal forces (B) and deformation diagrams (C).

moments and axial forces. The following three state functions were considered as a reasonable approach:

$$Z_{yield;land} = f_y - \max\left(\frac{\theta_M M_{wall}(z)}{W_{wall;land}(z)} + \frac{\theta_N N_{tube}(z)}{A_{tube}(z)}\right) \quad (5)$$

$$Z_{yield;water} = f_y - \max\left(\frac{\theta_M M_{wall}(z)}{W_{wall;water}(z)} - \frac{\theta_N N_{tube}(z)}{A_{tube}(z)}\right) \quad (6)$$

$$Z_{buckling} = M_{Rd} - M_{Ed} = min\left(\theta_B f_B f_y W_{tube}(z)\left(1 - \left(\frac{\theta_N N_{tube}(z) L_s}{N_{Rd}(z)}\right)^{1,7}\right) - \theta_M M_{wall}(z) L_s\right) \quad (7)$$

Where:

$$f_B = 1.573e^{\frac{-0.0021 D_{tube} f_{y;measured}}{t_{tube} f_{y;ref}}} \quad (8)$$

And where:

$Z_{yield;land}$ State function, maximum stress in outer fiber of combi-wall on landside [kN/m^2]
$Z_{yield;water}$ State function, maximum stress in outer fiber of combi-wall on waterside [kN/m^2]
$Z_{buckling}$ State function, local buckling of tube [kNm/m^1]
f_y Yield strength includes both variability and model uncerainty [kN/m^2]
$f_{y;measured}$ Measured yield strength during full-scale tests [kN/m^2]
$f_{y;ref}$ Reference yield strength in accordance with EN1993 [31,41], [kN/m^2]
M_{wall} Bending moment in combi-wall [kNm/m^1]
N_{tube}Axial force at position of maximum bending moment in combi-wall [kNm/m^1]
F_{anchor} Anchor force [kN]
$W_{combi\text{-}wall}$ Section modules, combi-wall [m^3/m^1]

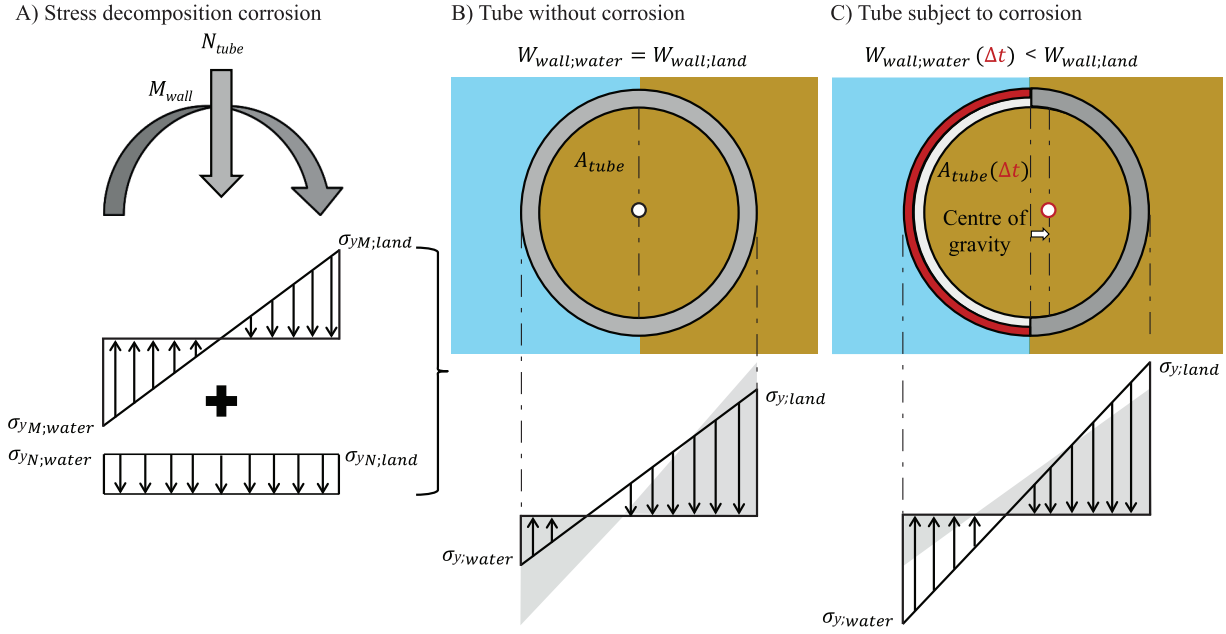

Fig. 6. Stress decomposition (A) over the cross-section of a combi-tube without (B) and subject to corrosion (C).

W_{tube} Section modules, combi-wall [m^3/m^1]
A_{tube} Sectional area tube [m^2/m^1]
M_{Ed} Maximum bending moment per pile [kNm]
M_{Rd} Reduced resisting bending moment per pile [kNm]
N_{Rd} Maximum resistance for axial compressive force per pile [kN]
L_s center-to-center distance, combi-wall system [m]
f_B Empirical formula based on experiments [41] [-]
N_{Rd} Maximum resistance for axial compressive force per pile [kN]
z Depth across height of combi-wall
ε Ratio of reference to nominal yield strengths, which equals $\sqrt{f_{y;ref} / f_y}$ [-]
θ_B Factor to account for model uncertainty related to buckling experiments [41] [-]
θ_M Factor to account for model uncertainty in bending moments [-]
θ_N Factor to account for model uncertainty in axial forces [-]

3.3. Distribution functions and correlations

This section presents the properties of the random variables used in this study (Table 1). The characteristic values employed comply with the original design [56], and for the most part the variation coefficients were determined in accordance with recommendations in literature [21]. Furthermore, time-dependent and time-independent random variables were taken into account. The methods used to perform the time-dependent reliability analysis are described in Section 3.4. The material properties and model uncertainty were considered to be time-independent variables, whereas water levels, operational loads and corrosion were assumed to vary over time.

The equivalent wall-thickness loss due to corrosion Δt_{eq} was modelled using Jongbloed's corrosion curves (Fig. 3B), which represent the mean value of uniform and pitting corrosion combined. It should be noted that these curves, which are based on millions of wall-thickness measurements, exhibit higher corrosion rates when compared with other design guidance [13,32]. To illustrate the influence of different corrosion environments, this study examines the effect of all nine corrosion curves on the annual failure rate in the permanent immersion zone. The uncertainty related to corrosion-induced degradation was estimated using field measurements from the port of Rotterdam [22]. The variation coefficients found for distinctive corrosion environments range between 0.1 and 0.5, which is in accordance with other literature [4,9,48,50]. The effect of the coefficient of variation on the reliability index was examined by performing a sensitivity analysis (Section 04.3).

Furthermore, the uncertainty in the corrosion rate was assumed to be fully correlated over time, since the experience with corrosion measurements is that the uncertainty is mainly epistemic in nature. In other words, the main uncertainty is usually which corrosion curve applies; but once the relevant curve has been determined using measurements, the development of corrosion mostly follows that curve throughout the quay wall's service life. In modeling terms, this means that the random variable representing the uncertainty in corrosion determines the position relative to the mean curve throughout the entire service life being considered. Mainly to prevent simulation of unrealistically high or low corrosion rates during the crude Monte Carlo analysis, the respective probability distribution function was truncated; the effect of that on the results of this study was negligible, as demonstrated in the sensitivity analysis (Section 0).

It is worth noting that the authors of this paper recently performed a finite element-based assessment of the reference quay wall concerned in this study. The reader is therefore referred to Roubos et al. [49] for a detailed description of other random variables.

Table 1
Type of distribution and variation coefficient used in the Blum-based reliability assessment.

Design parameter	Time-dependent	SI	X_k	μ	Distribution	*Variation coefficient V*
Unit weight of soil γ_{sat} [h]					Normal[21]	0.05[41] [55], [62],
- Backfill (1)	No	kN/m^3	20.0	20.0		
- Reclamation sand (2)	No	kN/m^3	20.0	20.0		
- Holocene sand (3)	No	kN/m^3	20.0	20.0		
- Clay layer (4)	No	kN/m^3	17.0	17.0		
- Pleistocene sand (5)	No	kN/m^3	20.0	20.0		
Friction angle φ'_{rep} [h]					Normal[21]	0.10[b] [40] [55], [62],
- Backfill (1)	No	°	32.5	38.9		
- Reclamation sand (2)	No	°	30.0	35.9		
- Holocene sand (3)	No	°	30.0	35.9		
- Clay layer (4)	No	°	22.5	26.9		
- Pleistocene sand (5)	No	°	32.5	38.9		
Cohesion c' [h]	No	kPa	5.0	6.9	Lognormal[21]	0.20 [40] [55], [62],
Yield strength f_y	No	N/mm^2	485	510	Lognormal[21]	0.07[41] [55], [21],
Tube diameter D_{tube}	No	m	1.067	1.067	Normal	0.05[a][21]
Wall thickness t_{tube}	No	m	0.15	0.15	Uniform	0.05[a][21]
Corrosion Δt_{eq}	Yes	m	n/a	variable[3]	Truncated normal[g]	0.50 [9] [22],
Outer water level (h_{OWL})	Yes	m	−0.84[d]	−0.84	Gumbel	0.20 m[e]
Ground water level (h_{GWL})	Yes	m	−0.34[d]	−0.34	Gumbel	0.25 m[e][18]
Annual maximum load Q_{t1}	Yes	kN/m^2	n/a	72.1	Gumbel	0.14
Lifetime maximum load Q_{t50}	n/a	kN/m^2	100	104.8	Gumbel	0.10 [10] [18], [19],, [40]
θ_B	No	–	n/a	1	Normal	0.20[c] [41]
θ_M	No	–	n/a	1	Lognormal	0.10[f]
θ_N	No	–	n/a	1	Lognormal[21]	0.10 [21]

[a] Based on production and execution tolerances, as well as project-specific acceptance criteria in the port of Rotterdam.
[b] By analogy with EN 1997 [33], considered at 5% strain rate [18].
[c] Depends on the selected corrosion curve.
[d] Outer water level is based on low low water at spring tide (LLWS); the groundwater level depends on the position of the drainage system. Water loads were considered as non-dominant loads, in accordance with the design report [56].
[e] Geometrical standard deviation Δ_a based on the water-level measurements [7].
[f] Factor is slightly lower than that recommended by the Probabilistic Model Code [21] for modeling plates, which is 0.2; this is because measurements showed that the models used are conservative rather than optimistic [2] [18], [61],.
[g] Truncated by neighbouring corrosion curves.
[h] Since the soil layers and failure mechanisms involved in the problem are relatively large compared to the vertical scale of fluctuation of soil parameters, it full spatial averaging in the vertical direction was assumed, and the random variables for soil properties reflect the uncertainty in layer average properties.

Table 2
Simplified correlation matrix.

	φ	γ_{sat}	c'	OWL	GWL	θ_M	θ_N
φ	–	0.50[a]	−0.65[a]	–	–	–	–
γ_{sat}	0.50[a]	–	−0.09[a]	–	–	–	–
c'	−0.65[a]	−0.09[a]	–	–	–	–	–
OWL	–	–	–	–	0.75[b]	–	–
GWL	–	–	–	0.75[b]	–	–	–
θ_M	–	–	–	–	–	–	1.00
θ_N	–	–	–	–	–	1.00	–

[a] Based on statistical analysis of a large dataset from Rotterdam [62].
[b] Approximated on the basis of statistical examination of the waterhead difference of a quay wall equipped with sensors in the port of Rotterdam [7]. This correlation is only valid when waterhead differences are non-dominant loads.

In addition, dependency between input variables was taken into account in order to prevent underestimation of the probability of failure. Table 2 presents the correlation matrix considered [49]. It is worth noting that the unsaturated (γ_{dr}) and saturated (γ_{sat}) soil weight densities were assumed to be fully dependent. This correlation was implemented automatically by applying a deterministic constant initial difference.

3.4. Numerical approach to time-dependent reliability analysis

This section describes the numerical approach to solve the time-dependent reliability problem. The solution to this problem was expressed as the probability of failure P_f. For each state function presented in Section 3.2, the probability of failure was defined as the probability of exceeding the limit state $g(X)=0$ [21]. In this study, the failure probability P_f was directly related to the reliability index β on the basis of Eq. (10) [11,15]. In addition, the conditional failure rate – which is defined as the probability of failure given that the structure has survived all previous years – was determined taking time-dependent effects on resistance $R(t)$ due to corrosion and variable loads $S(t)$ into account. When the instantaneous probability density functions of $R(t)$ and $S(t)$ are known, the instantaneous probability of failure $P_f(t)$ can be estimated. The basic formulation of the time-variant reliability problem is as follows:

$$g(X(t)) = R(t) - S(t) \tag{9}$$

$$P_f(t) = P(g(X(t)) \le 0) = \int_{g(X(t))\le 0} f_{X(t)}(x(t))dx(t) \tag{10}$$

$$P_f(t) = \Phi(-\beta(t)) \tag{11}$$

Where:

$g(X)$ State function of variable X
X Vector of random variables
$R(t)$ Resistance function at time t
$S(t)$ Solicitation or load function at time t
$P_f(t)$ Probability of failure at time t, assuming that the structure has survived until time t [-]
$f_X(x)$Joint probability density function of the vector X of random variables [-]
βReliability index [-]

This time-variant reliability problem was solved by performing a crude Monte Carlo analysis [2] and a first-order system reliability analysis. These reliability methods are further described in this section.

Crude Monte Carlo

The evolution of the annual probability of failure $P_{f,i}$ was examined for different scenarios using a Blum-based crude Monte Carlo analysis. For each year the conditional probability of failure in year i was derived, which is defined as the probability that failure occurs during year i given that the structure has survived until time t.

$$P_{f,i|S} = P(F_i|S_1 \cap ... \cap S_{i-1}) \tag{12}$$

Where:

$P_{f,\ i|S}$Discrete probability of failure per year i, given that the structure has survived all previous years [-]
F_iFailure in year i [-]
S_iSurvival in year i [-]

Analogous to equation Eq. (12), the cumulative probability of failure for the service life was determined using Eq. (13) and Eq. (14).

$$P_{f;t_n} = \sum_{i=1}^{n} P_{f,i|S} P_{S_{i-1}} \approx \sum_{i=1}^{n} P_{f,i|S} \tag{13}$$

$$P_{f;t_{sur}} = \sum_{i=1}^{n_{sur}} P_{f,i|S} P_{S_{i-1}} \approx \sum_{i=1}^{n_{sur}} P_{f,i|S} \tag{14}$$

$$P_{f;t_{rem}} = P_{f;t_n|S_{0..t_{sur}}} \approx P_{f;t_n} - P_{f;t_{sur}} \tag{15}$$

Where:

$P_{f;t_n}$Probability of failure in the interval [0, t_n) [-]
$P_{f;t_{sur}}$Probability of failure in the interval [0, t_{sur}) [-]
$P_{f;t_{rem}}$Probability of failure in the interval (t_{sur}, t_n) [-]
$S_{0..t_{sur}}$Survival in the interval [0, t_{sur}) [-]
t_n Service life, for new structurers this is the design lifetime and for existing structures the service life [years]
t_{sur} Period survived in the service life [years]
t_{rem} Remaining lifetime [years]
n Number of years in service life [-]
n_{sur} Number of years survived [-]

Practical application of crude Monte Carlo

In each simulation, the time-independent variables (Section 3.3) were generated once. In the case of time-dependent load variables, new stochastically independent values were generated for each year of the service life. The time-dependent wall thickness, or in other words the increase of corrosion, was considered fully correlated in time and it is based on a specific corrosion curve (Fig. 3). The crude Monte Carlo approach to solve the time-variant reliability problem starts by generating 10 million samples for the first year. The failures F_1 were used to estimate the annual failure rate $P_{f,\ 1|S}$. Subsequently, only the survivals S_1 that did not cross the limit state continued to year two. Starting from the second year, the time-independent variables remained unchanged, whereas new samples were generated for time-dependent variables such as corrosion Δt_{eq} and the variable load Q_{t1}. Again, the failures F_2 determine the annual failure rate $P_{f,\ 2|S}$. This process subsequently removes implausible realisations from the simulation (i.e. realisations in which the model predicts failure whereas the structure is supposed to survive) and was repeated for each year of the service life.

As an example, Fig. 7 presents the number of failures estimated on the basis of crude Monte Carlo. For this study, a service life of 75 years was assumed and consequently a total of approximately 750 million Blum-based evaluations were performed for each corrosion curve. However, Fig. 7 shows that the numerical noise for the situation without corrosion is still fairly high. This is because 750 million samples are too few to accurately calculate the failure rates in all individual years.

First-order system reliability analysis

In addition to crude Monte Carlo, a first-order approximation was performed to describe the development of the failure rate more accurately for fairly low failure rates. The annual failure rate (Eq. (12)) was reformulated by Eq. (16), where the failures F_i are conditional on the survivals S, which represents several survival events S_i [39].

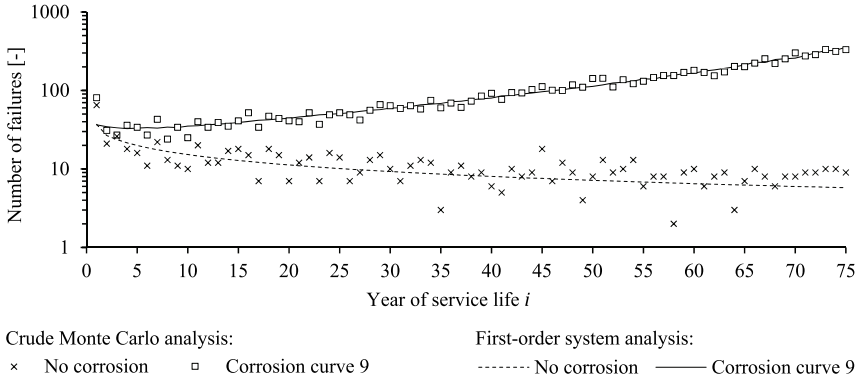

Fig. 7. Example of failure estimates obtained by performing a crude Monte Carlo and a first-order system reliability analysis for a service-proven quay wall.

$$P_{f,i|S} = \frac{P(F_i \cap S_1 \cap S_2 \cap \ldots \cap S_{i-1})}{P(S_1 \cap S_2 \cap \ldots \cap S_{i-1})} = \frac{P(g(X_i) \leq 0 \cap g(X_1) > 0 \cap g(X_2) > 0 \cap \ldots g(X_{i-1}) > 0)}{P(g(X_1) > 0 \cap g(X_2) > 0 \cap \ldots \cap g(X_{i-1}) > 0)} \quad (16)$$

Where,

$X_i = X\ (t_i)$Vector of random variables for year i

Since some dominant random variables are time-independent, the failures F_i and survivals S correlate to some extent. The numerator and the denominator of Eq. (16) were therefore solved using *FORM*, taking into account the correlation between individual events. The system of correlated limit state functions has a different vector of random variables X, which were solved by performing a first-order parallel system reliability analysis [29,52]. Fig. 7 shows the results of the first-order system reliability analysis. A more accurate method to solve Eq. (16) is the 'equivalent planes method' [44].

3.5. Finite-element-based calibration of Blum's method

Recent developments have shown that advanced finite element models of soil retaining walls can be successfully coupled to reliability tools [5,9,49,60]. However, performing a finite element-based Monte Carlo analysis requires too much calculation effort and was not feasible within the framework of this study. It was therefore decided to model the reference quay wall (Fig. 5) using Blum's analytical method [8,57]. This method analytically searches for equilibrium, while performing a plasticity analysis to estimate the horizontal stresses in the soil (Eq. (17) and Eq. (18)) [6,8]. Since Blum's method has some limitations, its outcome was evaluated using the finite element model Plaxis. This section discusses the calibration between Blum and the Plaxis hardening soil model.

$$K_{a;h} = \frac{\cos^2(\varphi)}{\left(1 + \sqrt{\frac{\sin(\delta+\varphi)\sin(\varphi)}{\cos(-\delta)}}\right)^2} \quad (17)$$

$$K_{p;h} = \frac{\cos^2(\varphi)}{\left(1 - \sqrt{\frac{\sin(\delta+\varphi)\sin(\varphi)}{\cos(-\delta)}}\right)^2} \quad (18)$$

Where:

$K_{a;h}$ Horizontal component of active earth-pressure coefficient [-]
$K_{p;h}$ Horizontal component of passive earth-pressure coefficient [-]
φAngle of internal friction [°]
δWall-friction angle [°]

The deterministic outputs of the two models were compared for design conditions (Fig. 5A). When using Blum's method, it is common practice to correct its calculation output [13] since this method overestimates the bending moments and underestimates the anchor force. The calculation output of the finite element model shows a small rotation and translation at the toe (Fig. 5C), whereas Blum assumes 'full fixation' of the combi-wall in the soil [26,53]. Moreover, Blum's method does not take into account vertical arching, assumes a rigid anchor support and neglects the structural rigidity of the combi-wall, as well as the backfilling of soil above the anchor. As a result, the bending moments and anchor forces derived using Blum are, respectively, higher and lower than those derived from the finite element model (Fig. 5A). The differences between the deterministic finite element-based and Blum-based calculations are within acceptable limits assuming $\delta = 0$ in combination with the following assumptions.

- The anchor force F_a calculated using Blum's method was increased by 15% [16].
- Blum's method does not return the normal force N_{wall}. Hence, this force was estimated using the Plaxis calculation output, which is approximately twice the horizontal anchor force F_a found using Blum.
- The maximum bending moment in the span M_{wall} was reduced by 30% [28,61].

In addition, the reliability index, the sensitivity factors and the design point found were also evaluated by performing Blum-based and finite element-based reliability assessments. The latter was undertaken using the reliability interface ProbAna® [49], in which the gradient-based *FORM* algorithm Abdo-Rackwitz [1] was selected. ProbAna® facilitates the coupling between Plaxis and the open-source probabilistic toolbox OpenTURNS [5]. Meanwhile, the Blum-based probabilistic analysis was conducted on the basis of the *FORM* and Monte Carlo. The *FORM* calculations are based on the Rackwitz-Fiessler algorithm [43] using the reliability tool Prob2B [3,4]. The results presented in the next section show that the reliability index, the design point and the associated sensitivity factors are quite similar.

4. Results

4.1. Comparison of Blum-based and FEM-based reliability assessment

This section compares the results of the reliability-based assessments performed using the analytical Blum model and the finite element model of the reference quay wall. It should be noted that this comparison does not yet take corrosion into account, since the main objective here is to compare the lifetime reliability indices β_{t50} associated with the cumulative failure probability $P_{f;t50}$ for a design lifetime of 50 years, as well as the annual reliability indices β_{t1} related to $P_{f,i}$. The results obtained show fairly small differences (Table 3), and hence modeling using the calibrated Blum's method seems a reasonable approach to reveal the effect of corrosion-induced degradation on the reliability of a quay wall.

Table 3
FoS, lifetime reliability index β_{t50} and annual reliability index β_{t1} for Z_{Yield} and $Z_{Buckling}$.

Design model		Reliability interface	Reliability method		$Z_{Yield;landside}$	$Z_{Yield;waterside}$	$Z_{Buckling}$
Plaxis	Finite elements	n/a	n/a	*FoS*	1.49	2.64	1.51
Plaxis	Finite elements	ProbAna®	FORM-AbdoRackwitz	$\beta_{t_{ref}}$	3.76[b]	5.33[b]	3.63[b]
Blum	Analytical	Prob2B®	FORM-RackwitzFiessler	$\beta_{t_{ref}}$	3.87	5.05	3.49
Blum	Analytical	Matlab	Monte Carlo	$\beta_{t_{ref}}$	3.74	4.94[a]	3.58
Plaxis	Finite elements	ProbAna®	FORM-AbdoRackwitz	β_{t_1}	4.39	5.79	n/a
Blum	Analytical	Prob2B®	FORM-RackwitzFiessler	β_{t_1}	4.44	5.68	3.84
Blum	Analytical	Matlab	Monte Carlo	β_{t_1}	4.36	5.18[a]	3.94

[a] The number of samples is too low to determine the reliability index; a more accurate result should be obtained with a higher number of samples.
[b] Results were derived in Roubos et al. [49].

In addition, the marginal differences in the *FoS* found by performing the allowable stress-based assessments also align with the marginal differences of the established reliability indices. The detailed results for Z_{yield} are presented in Appendix A.

4.2. Influence of corrosion on the FoS and the reliability index β

Corrosion-induced degradation reduces the *FoS* and reliability index β of the structural limit states. When assessing corroded combi-walls, the highest stresses typically develop in the permanent immersion zone (Fig. 3A). For the reference quay wall, this zone corresponds with corrosion curve 3 (Section 5.1); Fig. 8 therefore presents its corresponding effect on the remaining *FoS* and the annual reliability index β. The *FoS* on the waterside is initially much higher than that on the landside due to the presence of axial force N_{tube} (Fig. 6). Furthermore, Fig. 8A shows that the *FoS* for yielding on the landside and local buckling are quite similar (overlapping). By contrast, the results shown in Fig. 8B indicate that the uncertainty in time-independent random variables significantly influences the limit state for local buckling of a service-proven quay wall, since the annual reliability index significantly increases in the early service period.

Fig. 9 shows the results of the Blum-based reliability assessment for the limit state yielding (Z_{yield}) on the landside; The main reason for focusing on this limit state is that it is well-known and is currently used in the allowable stress-based assessments of corroded quay walls (Section 2). The annual failure rates and the associated annual reliability index were determined using crude Monte Carlo for all nine corrosion curves, as well as for the situation without corrosion. Furthermore, the trendlines of the corrosion curves are based on a first-order system analysis (Section 3.4). Given stationarity in the load variables, the results clearly illustrate that the annual failure rate is not constant (Fig. 9). During its early years of service, the annual failure rate of a service-proven quay wall shows a downward trend, which is the result of a decrease in epistemic uncertainty due to successful resistance to past service loading [14,59]. With low corrosion rates, the annual failure rate keeps decreasing throughout the first 75 years, whereas with higher corrosion rates the annual failure rate will start increasing at some point during this time.

Fig. 10A shows the impact of corrosion on the *FoS*. As expected, the *FoS* decreases due to wall-thickness loss, which is directly related to the service life using the corrosion curves (Fig. 3). When a quay wall is undamaged, the *FoS* remains constant (Fig. 10A) while the cumulative probability of failure of a service-proven uncorroded quay wall increases slightly over time (Fig. 10C). This indicates that the allowable stress-based method is only related to the reference period t_{ref} via the corrosion curves, while a change in service period always results in a change in $P_{f;t_n|S}$; This is because unfavorable time-dependent variables, such live loads, are more likely to occur during a longer service period.

In addition, Fig. 10B shows that the annual reliability index for all curves increases in the early period of service due to past service performance. For the situation without corrosion and for corrosion curve 3, the annual reliability index keeps increasing as the quay wall ages successfully, whereas curves 6 and 9 show already show a decrease.

If we assume that the quay wall's service life is 75 years and that it has survived all previous service loads, its residual cumulative probability of failure for its remaining lifetime can be determined. Fig. 10D shows that, despite corrosion, the residual cumulative probability of failure for a service-proven quay wall will decrease. When its remaining service life becomes short, e.g. $t_{rem} < 10$ years, Fig. 10D shows an exponential decrease in the cumulative probability of failure. This is a direct consequence of the

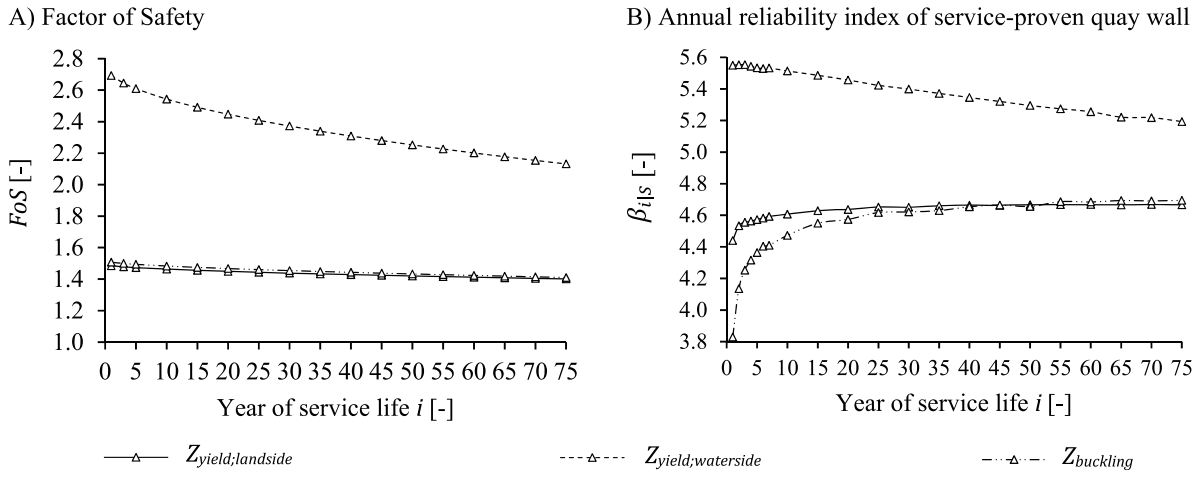

Fig. 8. Development of FoS (A) and annual reliability index (B) for Z_{yield} and $Z_{buckling}$ of a service-proven quay wall subject to corrosion curve 3 in the permanent immersion zone. The annual reliability curves are based on the first-order system analysis.

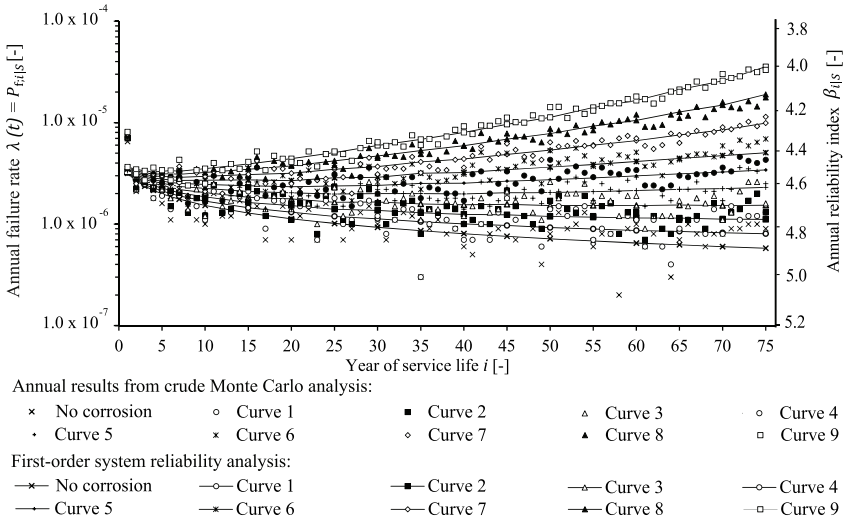

Fig. 9. Evolution of annual failure rate for different corrosion curves for the $Z_{yield;landside}$ in the permanent immersion zone.

decrease in uncertainty with regard to time-dependent variables, which play a much more dominant role in the remaining uncertainty compared with the uncertainty present during the design stage. Since unfavorable variable loads are less likely to occur during a shorter period of time, then where it has a successful service history the remaining cumulative probability of failure of a quay wall will decrease accordingly.

4.3. Sensitivity analysis

This sensitivity analysis aims to reveal the impact of the variation coefficient of important random variables – such as the angle of internal friction φ (Fig. 11A), the surcharge loads Q_{t1} (Fig. 11B), the yield strength f_y (Fig. 11C) and corrosion Δt_{eq} (Fig. 11D) – on the conditional annual

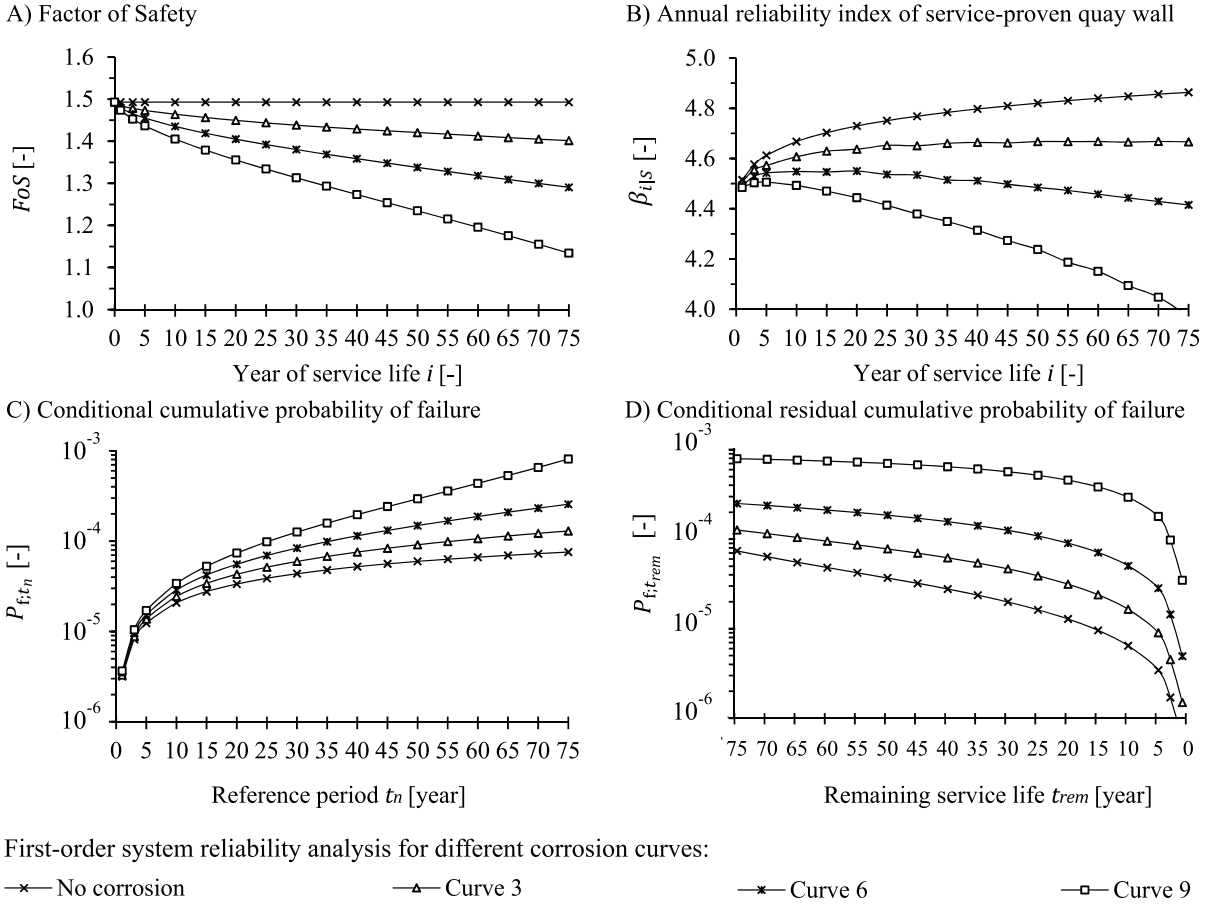

Fig. 10. Remaining factor of safety (A), development of annual reliability index (B), development of cumulative probability of failure (C) and remaining cumulative probability of failure (D) for $Z_{yield;landside}$ of a service-proven quay wall in the permanent immersion zone.

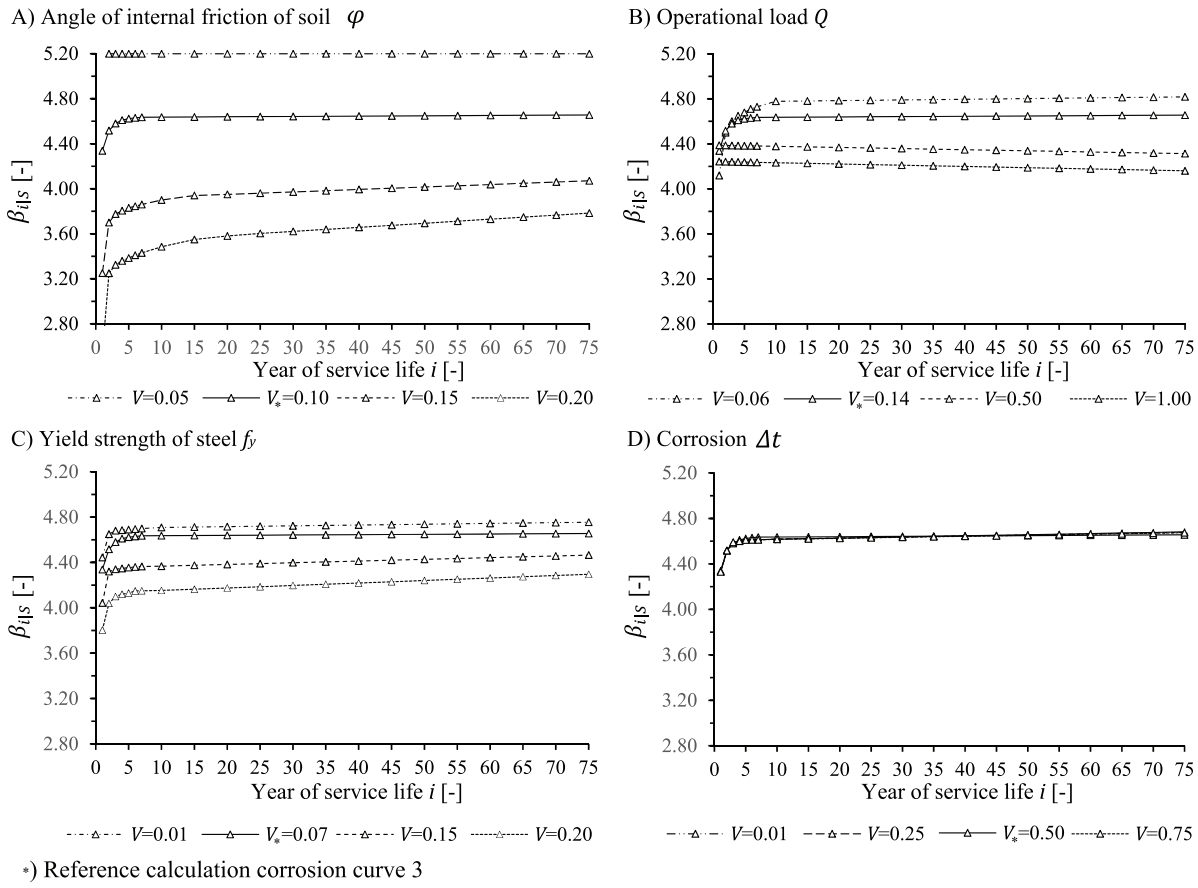

Fig. 11. Influence of variation coefficient of the soils' friction angle (A), surcharge load (B), yield strength (C) and corrosion (D) on the annual reliability index of a service-proven quay wall subject corrosion curve 3 in the permanent immersion zone. Trendlines are based on a crude Monte Carlo analysis.

reliability index. Vrijling and Van Gelder [59] concluded that the failure rate is largely influenced by uncertainties that have many realisations (such as environmental or operational loads) and uncertainties that only have one realization (e.g. soil conditions and material properties) during the service life. In general, small variations in strength properties of soil have a higher impact on the annual reliability index than small variations in loads, yield strength and corrosion-induced degradation. Since the curves found overlap, Fig. 11D illustrates that the variation coefficient of corrosion has almost no influence on the outcomes. This can be explained by a fairly low sensitivity factor, e.g. approximately 0.05 for Δt_{eq} (see Appendix B). Furthermore, it was found that replacing the truncated normal with a normal distribution function had negligible effect on the outcome. The reader is referred to Appendix B for the comparison with and without truncated distribution function.

The variation coefficient of the soils' internal friction angle was directly applied to its expected value in order to determine the standard deviation, while the characteristic value for the live load was considered to be invariant, representing a return period of 50 years.

In addition, Fig. 11A and Fig. 11B shows that the annual reliability index will become practically constant if Z_{yield} is dominated by uncertainty in time-dependent variables (many realisations during the service life and failures in subsequent years are independent [59]). By contrast, when time-independent random variables (one realization during the service life and failure in subsequent years are dependent [59]) are dominant, the annual reliability index will increase during the early years of service. Furthermore, Fig. 11B shows that a relatively small coefficient of variation for live loads only leads to a lower annual reliability index during the early service period. This is because the uncertainty in the live load Q_{t1} does not significantly influence the annual reliability indices – or, in other words, because the time-independent variables are dominant. Nevertheless, all the curves show higher annual reliability indices for lower variation coefficients of random variables, which is the direct result of a general decrease in the amount of uncertainty present in the reliability problem.

In general, the variation coefficient of random variables will determine the degree to which the reliability problem is time-variant, and hence whether the failure rate in the first or the final year of the service life will prevail. This is discussed further in the next section.

5. Discussion

5.1. Influence of corrosion on FoS and β of reference quay wall

Since the corrosion rate of the reference quay wall corresponds with corrosion curve 3 in the permanent immersion zone (Fig. 3A), this section describes the impact of that curve on the *FoS* and *β*. Also discussed are the results obtained for non-deteriorated, service-proven quay walls, in order to be able to better interpret the influence of wall-thickness loss on the reliability of a quay wall.

When an uncorroded quay wall has shown the ability to function during a certain time period, our confidence in its actual reliability level will increase. This is because it will be less likely that the strength properties of soil or steel, which show high sensitivity factors (Appendix A), are unfavorable. For quay walls subject to corrosion, this favourable effect will also be present. However, the quay wall's reliability level will also be negatively influenced by corrosion-induced degradation.

The annual failure rate of a service-proven quay wall subject to corrosion curve 3 (Fig. 9) still shows a slightly downward trend after 75 years of successful service history. Successful service seems to reduce the remaining time-independent uncertainty. Consequently, it is unlikely that

the end of the service life of this quay wall will be reached due to corrosion in the first 75 years. In this regard, the presence of the normal force induced by the vertical component of anchor force plays a crucial role. It ensures that the stresses on the landside prevail over those on the waterside (Fig. 8). For quay walls without inclined anchors, it is highly likely that stresses on the waterside rather than the landside will determine the end of their service life. Furthermore, the annual reliability index (Fig. 10B) of service-proven quay walls exposed to high corrosion rates, as in corrosion curves 6 and 9, will therefore continue to decrease.

5.2. Influence of remaining service life on probability of failure of service-proven quay walls

The annual failure rate found in this study generally shows a downward trend in the early years of service (Fig. 8B). However, the further evolution of the failure rates depends on the rate of corrosion and the number of years survived. When assessing quay walls, therefore, either the first or the last year of the service life will prevail, for low and high corrosion rates respectively. The reference period of new quay walls is presently based on a design lifetime of 50 years, which is quite arbitrary. Changing this reference period will directly affect the cumulative probability of failure (Fig. 10C), since the presence of higher loads and a higher degree of deterioration are more likely during a longer period of time. Furthermore, the uncertainty of time-independent variables such as soil or yield strength is not significantly affected by changing the reference period. In fact, the presence of fairly unfavorable time-independent variables becomes increasingly unlikely as a quay wall ages successfully.

When assessing a service-proven quay wall, it is possible to predict the end of its lifetime and the associated remaining service life. But this requires adjustment of the reference period. If we assume that a quay will be replaced after 75 years of service, for instance, we can determine the remaining cumulative probability of failure given its successful past performance (Fig. 8D). Since reliability is always related to a certain reference period, and the remaining service lives of different existing quay walls will probably differ, deriving reliability targets for the remaining lifetime does not seem very efficient. In general, it appears more practical to evaluate reliability on an annual basis rather than for longer time periods, since the latter will introduce an iterative procedure to determine the remaining service life.

5.3. Evaluation of allowable stress-based method to assess corroded combi-walls

Before discussing the allowable stress-based method to assess corrosion-induced degradation of combi-walls (Section 1.2), it is worth noting that neither yielding nor local buckling failures have been identified in practice. This indicates that the method is rather conservative, a finding also supported by the decrease found in the annual failure rate (Fig. 9). Moreover, the allowable stress-based method presently features the assessment of single structural members, e.g. one tube in a combi-wall system. However, a combi-wall system generally has a some additional capacity to redistribute internal forces. As a result, it is almost impossible that only a single combi-tube will show yielding or local buckling. This redistribution has not yet been taken into account. Furthermore, despite the allowable stress-based method already distinguishing different corrosion zones across the height of the combi-wall (Fig. 3A), it neglects spatial variation along the quay wall. It is therefore highly recommended that horizontal correlation lengths in the different corrosion zones be studied, because it seems unlikely that multiple tubes will show the same amount of pitting corrosion at the exact same position. Hence, it is expected that the actual reliability level of combi-walls is significantly higher.

Example

The differences between the allowable stress-based method and the probabilistic approach can best be discussed by presenting an example. However, our reference quay wall is subject to the relatively low corrosion rates of curve 3 and as a result its likely service lifetime is well beyond 75 years. Consequently, the end of the lifetime of the reference quay wall was predicted using the results from the more conservative corrosion curve 9, predominantly to demonstrate the differences and also to show the possible impact of corrosion on the stresses on the waterside. Predictions on the basis of the allowable stress approach show that the stresses on the waterside after approximately 50 years become higher than those on the landside, whereas following the probabilistic method shows that this is already likely after approximately 40 years (Fig. 12). Furthermore, the minimum required *FoS* is reached after 49 years. If we assume that the reference quay wall corresponds with RC1 of EN 1990 [30], the minimum annual target reliability index is exceeded after 72 years (

Table 4). In other words, using the probabilistic approach results in an increase of the remaining service life of approximately 35%. In addition, the residual cumulative probability of failure for the last three years is 2.85, which is higher than the minimum target reliability indices presented in literature [33,34,48,50]. This example illustrates the potential benefits of performing reliability-based assessments to safely extend the lifetime of service-proven quay walls. However, it should be noted that accidental load combinations, such as earthquake-induced ground motion and extreme tidal waterhead differences, were not taken into consideration in the present investigation. Where loading events are infrequent, satisfactory past performance may not be a good indicator [39]. Furthermore, for soil-retaining walls that are part of another system, such as a flood-defense system, the length effect need to be taken into consideration [10,45].

6. Conclusion and recommendations

The results of this study show the effect of corrosion-induced degradation on the reliability of service-proven combi-walls. Its most important findings are as follows:

- Annual failure rates and the associated reliability indices of service-proven quay walls are largely time-dependent. The failure rate of non-deteriorating quay walls decreases over time. For quay walls with successful service histories and subject to low corrosion rates, the highest annual reliability indices were typically observed in the first year of the service life, while for higher corrosion rates the final year is critical.
- The allowable stress-based method of assessing corrosion-induced degradation of combi-walls is conservative rather than optimistic in the case of service-proven quay walls.
- The ratio between the factor of safety and the reliability index changes over time and depends on the corrosion rate and the number of years survived. Hence, no generally applicable relationship was found.
- The reliability assessments performed using the calibrated Blum model show results similar to those from finite element-based reliability assessments.
- The variation coefficient of the angle of internal friction significantly influences the evolution of the annual failure rate over time.

Successful service, i.e. the survival of service loads, enables us to reduce time-independent uncertainties [14] such as uncertainty in soil strength of quay walls, leading to an increase in reliability. However, this positive effect will be less pronounced for quay walls exposed to rare extreme events such as earthquakes or accidental loading. Hence, it is highly recommended that further investigation be undertaken into the influence of extreme events and accidental load combinations.

A reference period of one year enables us to evaluate quay-wall reliability, while taking into account the effects of past performance and degradation. Moreover, within a one-year reference period, the effects of past performance and degradation can be taken into account in an appropriate

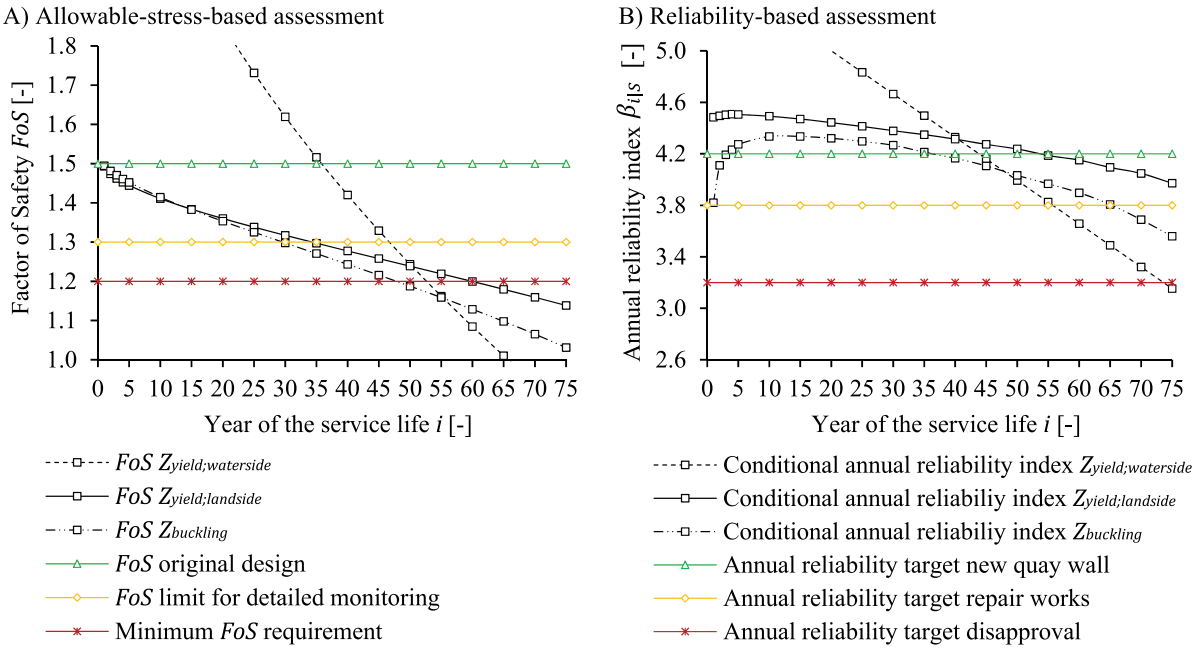

Fig. 12. Comparison of allowable stress-based (A) and reliability-based (B) assessments of a service-proven quay wall subject to corrosion curve 9 in the permanent immersion zone.

manner. These findings can play an important role in the evaluation of the reliability of an existing quay wall, since then its remaining service life and the associated reference period are generally unknown a priori. Hence, using annual target reliability indices is preferred.

Based on the findings of this study, the early application of a test load close to the characteristic/design load applied directly after completion of the structure can be an effective strategy to increase its reliability during its remaining service life [15,39]. The application of such a test load in a pre-posterior analysis is therefore recommended. And if the outcomes are favourable in cost-benefit terms, so is the development of full-scale test protocols for new and service-proven quay walls.

Furthermore, this study has shown that a calibrated Blum-based crude Monte Carlo analysis gives quite similar results to the finite-element-based *FORM* approximation. It would therefore be very interesting to compare these results with those obtained from other reliability methods, e.g. using response surfaces (a.k.a. surrogate models) such as kriging [54] or directional adaptive response surface sampling (DARS) [25], in order to verify the applicability of such methods for finite element-based and time-dependent reliability assessments.

In addition, further study of the development of pitting corrosion over time (position and propagation) [27,36] is recommended, as is work to clarify how the combination of uniform and pitting corrosion can be taken into account when assessing combi-walls, e.g. by applying random field theory. Moreover, we suspect that truncating the probability distribution of corrosion does not always have a negligible effect on the outcome. This effect is probably much greater for sheet pile walls than for combi-walls, and hence we recommend that this aspect be studied in more detail and do not recommend truncation of the corrosion uncertainty as general practice.

Finally, the results of this study show that time-independent uncertainty decreases during the early years of a quay wall's service life. This finding can play a crucial role in the assessment of existing quay walls, and presumably in that of all other service-proven geotechnical structures. It is therefore highly recommended that practical guidelines be further developed, e.g. by updating the initial estimates of time-dependent random variables, in order to safely extend the service life of existing quay walls and other structures with similar features.

CRediT authorship contribution statement

Alfred A. Roubos: Conceptualization, Methodology, Visualization, Investigation, Formal analysis, Writing - original draft. **Diego L. Allaix:** Methodology, Investigation, Formal analysis, Writing - review & editing. **Timo Schweckendiek:** Writing - review & editing. **Raphael D.J.M. Steenbergen:** Writing - review & editing, Supervision. **Sebastiaan N. Jonkman:** Supervision, Writing - review & editing.

Declaration of Competing Interest

The authors declare that there are now conflicts of interest.

Acknowledgements

On behalf of Delft University of Technology, the Port of Rotterdam, TNO and Deltares, the authors would like to thank all the companies and organisations involved in this study – and SmartPort in particular – for their support, funding and hospitality. Special thanks go to Mr A. P. Louwen and Mr B. P. Jongbloed of the Port of Rotterdam Authority, who

Table 4
Exceeding of safety limits and annual reliability targets on the basis of the allowable stress and reliability-based assessments, respectively.

Allowable stress-based	$Z_{yield;landside}$	$Z_{yield;waterside}$	$Z_{buckling}$	Reliability-based	$Z_{yield;landside}$	$Z_{yield;waterside}$	$Z_{buckling}$
New design; $FoS < 1.5$	Year 1	Year 36	Year 1	New design; $\beta < 4.2$ [30] [33],	Year 50	Year 43	Year 38
Intensive monitoring; $FoS < 1.3$	Year 35	Year 47	Year 29	Repair works; $\beta < 3.8$ [48]	> Year 75	Year 56	Year 66
Disapproval; $FoS < 1.2$	Year 61	Year 53	Year 49	Disapproval; $\beta < 3.2$ [48]	> Year 75	Year 72	> Year 75

provided detailed insights into the method used to assess corrosion-induced degradation in the port of Rotterdam. Mr H. Brassinga is gratefully acknowledged for sharing his knowledge and for reviewing the Plaxis model used. The support of Mr J. Plugge was of great help in correctly interpreting and calibrating Blum's method. Development of the limit state function for local buckling would not have been possible without the help of Dr D. J. Peters, who also reviewed this paper on behalf of RH-DHV and Delft University of Technology. Finally, Ms A. Laera and Dr R. Brinkgreve of Plaxis company are gratefully acknowledged for their contribution to the development of the ProbAna® reliability interface.

Appendix A. . Comparison of reliability methods

Table A1

Table A1
Comparison of Blum&Prob2B with Plaxis & OpenTURNS [49] in respect of lifetime reliability index, the design points in physical space X* and normal space U* and the sensitivity factor α for $Z_{yield;landside}$.

		Blum & Prob2B			Plaxis & OpenTURNS [49]		
Reliability index β		3.87			3.77		
Parameter	***SI***	***X****	***U****	$\alpha_{u\text{-}space}$	***X****	***U****	$\alpha_{u\text{-}space}$
$E_{50;Backfill}$	*mPa*	n/a	n/a	n/a	47.9	−0.12	−0.03
$E_{50;\ Reclamation}$	*mPa*	n/a	n/a	n/a	25.6	−0.70	−0.19
$E_{50;\ Holocene}$	*mPa*	n/a	n/a	n/a	24.7	−0.88	−0.23
$E_{50;\ Clay}$	*mPa*	n/a	n/a	n/a	4.8	−0.09	−0.02
$E_{50;Pleistocene}$	*mPa*	n/a	n/a	n/a	47.6	−0.15	−0.04
$\varphi_{\ Backfill}$	°	39.4	0.13	0.03	39.7	0.26	0.07
$\varphi_{\ Reclamation}$	°	33.1	−0.78	−0.20	29.2	−1.74	−0.46
$\varphi_{\ Holocene}$	°	24.7	−3.11	−0.80	28.4	−1.93	−0.51
$\varphi_{\ Clay}$	°	26.6	−0.12	−0.03	27.5	0.24	0.06
$\varphi_{\ Pleistocene}$	°	38.6	−0.06	−0.02	39.7	0.26	0.07
$\gamma_{sat;\ Backfill}$	*kPa*	20.3	0.32	0.08	20.2	0.20	0.05
$\gamma_{sat;\ Reclamation}$	*kPa*	20.0	0.45	0.12	19.2	−0.23	−0.06
$\gamma_{sat;\ Holocene}$	*kPa*	17.8	−0.77	−0.20	18.5	−0.36	−0.10
$\gamma_{sat;\ Clay}$	*kPa*	17.0	0.00	0.00	17.1	0.11	0.03
$\gamma_{sat;\ Pleistocene}$	*kPa*	20.0	0.01	0.00	20.0	−0.02	−0.00
h_{OWL}	*m*	−0.82	0.06	0.01	−0.83	0.06	0.02
h_{GWL}	*m*	−0.27	−0.24	−0.06	−0.29	−0.25	−0.07
Q_{t50}	kN/m^2	116	1.12	0.29	112	0.56	0.15
$h_{retaining}$	*m*	n/a	n/a	n/a	0.23	−0.66	−0.18
t_{tube}	*mm*	14.6	−0.53	−0.14	14.3	−0.91	−0.24
D_{tube}	*m*	1.029	−0.72	−0.19	1.035	−1.03	−0.27
f_y	N/mm^2	479.7	−0.84	−0.22	503.5	−0.72	−0.19
θ_M[1]	–	1.10	0.96	0.25	1.15	1.52	0.40
θ_N[1]	–	1.02	0.24	0.06	1.03	0.33	0.09

The model uncertainties $\theta_M$and θ_N are assumed to be independent.

Appendix B. . Comparison with and without truncation

TABLE A2

Table A2
Comparison between truncated normal distribution and normal distribution in respect of lifetime reliability index, the design points in physical space X* and normal space U* and the sensitivity factor α for corrosion curve 3 of $Z_{yield;landside}$.

		Truncated normal distribution for Δt_{eq}			Normal distribution for Δt_{eq}		
Reliability index β		4.30			4.29		
Parameter	***SI***	***X****	***U****	$\alpha_{u\text{-}space}$	***X****	***U****	$\alpha_{u\text{-}space}$
$\varphi_{\ Backfill}$	°	39.5	0.15	0.03	39.4	0.12	0.03
$\varphi_{\ Reclamation}$	°	33.1	−0.78	−0.18	32.9	−0.82	−0.19
$\varphi_{\ Holocene}$	°	24.1	−3.29	−0.77	24.1	−3.28	−0.76
$\varphi_{\ Clay}$	°	26.6	−0.13	−0.03	26.6	−0.13	−0.03
$\varphi_{\ Pleistocene}$	°	38.6	−0.06	−0.01	38.5	−0.08	−0.02
$\gamma_{sat;\ Backfill}$	*kPa*	20.4	0.38	0.09	20.4	0.36	0.08
$\gamma_{sat;\ Reclamation}$	*kPa*	20.0	0.50	0.12	20.0	0.49	0.12
$\gamma_{sat;\ Holocene}$	*kPa*	17.6	−0.85	−0.20	17.6	−0.85	−0.20
$\gamma_{sat;\ Clay}$	*kPa*	16.9	−0.01	−0.01	17.0	0.01	0.00
$\gamma_{sat;\ Pleistocene}$	*kPa*	20.0	−0.01	−0.01	20.0	0.01	0.00
$c_{\ Clay}$	*kPa*	6.66	−0.00	−0.00	6.64	−0.01	−0.00
h_{OWL}	*m*	−0.83	0.13	0.03	−0.83	0.14	0.03
h_{GWL}	*m*	−0.28	−0.29	−0.07	−0.28	−0.28	−0.06
Q_{t1}	kN/m^2	90.5	1.54	0.36	89.8	1.49	0.35
t_{tube}	*mm*	14.36	−0.66	−0.15	14.36	−0.66	−0.15
D_{tube}	*m*	1.029	−0.73	−0.17	1.028	−0.72	−0.17
f_y	N/mm^2	478	−0.89	−0.21	478	−0.89	−0.21
θ_M	–	1.13	1.27	0.30	1.13	1.27	0.30
θ_N	–	1.13	0.00	0.00	1.13	0.00	0.00
Δt_{eq}		3.12	0.16	0.04	3.52	0.35	0.08

References

[1] Abdo T, Rackwitz R. A new beta-point algorithm for large time-invariant and time-variant reliability problems. Proceedings of the 3rd IFIP WG7.5 working conference on reliability and optimisation of structural systems. Berlin, Germany: Springer; 1991. p. 112.

[2] Adel N. Load testing of a quay wall: an application of Bayesian updating. MSc thesis Delft, The Netherlands: Delft University of Technology; 2018.

[3] Allaix D, Steenbergen RDJM, Wessels JFM. Target reliability levels for the design of quay walls. Delft, The Netherlands: TNO; 2017.

[4] Allaix D, Steenbergen RDJM, Wessels JFM. Target reliability levels for existing quay walls. Delft, The Netherlands: TNO; 2018.

[5] Andrianov G, Burriel S, Cambier S, Dutfoy A, Dutka–Malen I, Rocquigny Ede, Sudret B, Benjamin P, Lebrun R, Mangeant F, Pendola M. Open TURNS, an open source initiative to Treat Uncertainties, Risks 'N Statistics in a structured industrial approach. Proceedings of the European safety and reliability conference 2007, ESREL 2007 – Risk, reliability and societal safety. 2. 2007.

[6] Bakker KJ. Soil Retaining Structures Doctoral thesis Delft, The Netherlands: Delft University of Technology; 2000

[7] Berg, van der J.W., Seesing, B.A.S., Greef J., Jaspers Focks, D.J., & Quist, P. (2018), *Quay Wall of the Future: Comparison Report*. Rotterdam, The Netherlands: Smart Port. RT780-49/18-007.302.

[8] Blum H. Einspannungsverhaltnisse bei bohlwerken. Berlin, Germany: W. Ernst und Sohn; 1931.

[9] Boero J, Schoefs F, Yanez-Godoy H, Capra B. Time-function reliability of harbour infrastructures from stochastic modelling of corrosion. Eur J Environ Civ Eng 2012;16:1187–201.

[10] Calle EOF, Spierenburg SEJ. Veiligheid van damwandconstructies – Onderzoeksrapportage deel 1, for cur committee C69. Delft, The Netherlands: Deltares; 1991. report CO-31690/12.

[11] Cornell CA. A probability-based structural code. ACI J 1969;66:974–85.

[12] Gijt JGde, Broeken ML. Quay walls. 2nd Edition Delft, The Netherlands: SBRCURnet; 2013. ISBN 987-1138000230.

[13] Grabe, J. (2012), *Recommendations of the Committee for Waterfront Structures, Harbours and Waterways EAU 2012*, ninth edition. Hamburg, Germany. ISBN 978-3433031100.

[14] Hall WB. Reliability of service-proven structures. Struct Eng 1988;114:608–24.

[15] Hasofer A, Lind N. An exact and invariant first-order reliability format. J Eng Mech 1974;100:111–21.

[16] Hoesch. Spundwand-Handbuch berechnung. Dortmund, Germany: Hoesch; 1977.

[17] Houyoux, C., Alberts, A., Heeling, A., Benaissa, B., & De Cristofaro, N. (2007), *Design Method for Steel Structures in Marine Environment Including the Corrosion Behaviour*. European Commission Report EUR22433EN. ISBN 927903768.

[18] Huijzer GP, Hannink G. The construction of parameterized subsurface models. Proceedings of the 11th European conference on soil mechanics and foundation engineering. 1995.

[19] Huijzer GP. Eindrapport probabilistische analyse damwand constructies. Rotterdam, The Netherlands: Port of Rotterdam Authority; 1996.

[20] ISO 2394. General principles on reliability for structures. Geneva, Switzerland: International Organisation for Standardisation; 2015.

[21] JCSS. Probabilistic model code. part 1. 2001. Joint Committee on Structural Safety www.jcss.byg.dtu.dk.

[22] Jong S. Technical report: corrosion and pitting on quay structures. Rotterdam, The Netherlands: Port of Rotterdam Authority; 2018.

[23] Jongbloed BP. End report: causes of corrosion in the port of rotterdam. Rotterdam, The Netherlands: City of Rotterdam; 2008.

[24] Jongbloed BP. From inspection to prediction of corrosion-induced degradation of quay walls in port of rotterdam. Rotterdam, The Netherlands: Port of Rotterdam Authority; 2019.

[25] Jonkman, S. N., .Steenbergen, R.D.J.M., Morales-Nápoles, O., Vrouwenvelder, A.C. W.M., & Vrijling, J.K. (2015), *Probabilistic Design: Risk and Reliability Analysis in Civil Engineering*. Delft, The Netherlands.

[26] Karamperidou A. Parametric Analysis of Quay Walls with Relieving Platform,by Means of Elastic Supported Beam and Finite Element Method MSc thesis Delft, The Netherlands: Delft University of Technology; 2018

[27] Kolios A, Srikanth S, Salonitis K. Numerical simulation of material strength deterioration due to pitting corrosion. Proc CIRP 2014;13:230–6.

[28] Leatemia, F.L., & Heijndijk, P. (1998), *Design Guideline: Quay Walls, Port of Rotterdam*. Rotterdam, The Netherlands.

[29] Lemaire M. Structural reliability. London, United Kingdom: Wiley; 2009. ISBN 978-1848210820.

[30] NEN–EN 1990. Eurocode 0 – Basis of structural design. Brussels, Belgium: European Committee for Standardisation; 2011.

[31] NEN-EN 1993-1. Eurocode 3: design of steel structures – Part 1-1: general rules and rules for buildings. Brussels, Belgium: European Committee for Standardisation; 2011.

[32] NEN-EN 1993-5. Eurocode 3: design of steel structures – Part 5: piling. Brussels, Belgium: European Committee for Standardisation; 2007.

[33] NEN–EN 1997. Eurocode 7: geotechnical design – Part 1: general rules. Brussels, Belgium: European Committee for Standardisation; 2004.

[34] NEN–EN 8700. Basis of structural assessment of existing structures – Buildings: the minimum safety level. Delft, the Netherlands: NEN; 2011.

[35] Melchers RE. Corrosion uncertainty modelling for steel structures. J Constr Steel Res 1999;52:3–19.

[36] Melchers RE, Jeffrey RJ. Probabilistic models for steel corrosion loss and pitting of marine infrastructure. Reliab Eng Syst Saf 2008;93:423–32.

[37] Melchers RE, Wells T. Models for the anaerobic phases of marine immersion corrosion. Corros Sci 2006;48:1791–811.

[38] Melchers RE. Long-term immersion corrosion of steels in seawaters with elevated nutrient concentration. Corros Sci 2015;81:110–6.

[39] Melchers RE, Beck AJ. Structural reliability analysis and prediction. Wiley; 2018. ISBN: 978-1119266075.

[40] Osório, P., Odenbreit, P., & Vrouwenvelder, T. (2010), Structural reliability analysis of quay walls with sheet piles. *PIANC MMX Congress*. Liverpool, United Kingdom.

[41] Peters DJ, Sadowski A, Rotter M, Taras A. Calibration of Eurocode design models of thin-walled cylinder under bending with full-scale tests. Eurosteel 2017 2017;1:3729–40.

[42] Phoon KK, Retief JV. Reliability of geotechnical structures in ISO239. CRC Press; 2016. ISBN 978-1138029118.

[43] Rackwitz R, Fiessler B. Structural reliability under combined random load sequences. Comput Struct 1997;9:489–94.

[44] Roscoe K, Diermanse F, Vrouwenvelder T. System reliability with correlated components: accuracy of the equivalent planes method. Struct Saf 2018;57:53–63.

[45] Roubos AA, Grotegoed D. Urban quay walls. Delft, The Netherlands: SBRCURnet; 2014. ISBN 978-1138000230.

[46] Roubos AA, Groenewegen L, Peters DJ. Berthing velocity of large seagoing vessels in the port of Rotterdam. Mar Struct 2017;51:202–19.

[47] Roubos AA, Steenbergen RDJM, Schweckendiek T, Jonkman SN. Risk-based target reliability indices of quay walls. Struct Saf 2018;75:89–109.

[48] Roubos AA, Allaix D, Fischer K, Steenbergen RDJM, Jonkman SN. Target reliability indices for existing quay walls derived on the basis of the LQI criterion. IALCC. 2018.

[49] Roubos AA, Schweckendiek T, Brinkgreve R, Steenbergen RDJM, Jonkman SN. Finite element-based reliability assessment of quay walls. Comput Geotech 2020. https://doi.org/10.1080/17499518.2020.1756344.

[50] Roubos AA, Allaix D, Fischer K, Steenbergen RDJM, Jonkman SN. Target reliability indices for existing quay walls derived on the basis of economic optimisation and human safety requirements. Structure and infrasstructure engineering. 2019.

[51] Schweckendiek T, Courage WMG, Gelder PHAJMvan. Reliability of sheet pile walls and the influence of corrosion – structural reliability analysis with finite elements. Proceedings of the European safety and reliability conference 2007 (ESREL 2007). 2007. p. 1791–9.

[52] Sørensen JD. Notes in structural reliability theory and risk analysis. Aalborg, Denmark: Institute of Building Technology and Structural Engineering; 2004.

[53] Steenepoorte C. Het ontwerp van een kademuurkonstruktie voor container overslag in de Amazonehaven op de Maasvlakte MSc thesis Delft, The Netherlands: Delft University of Technology; 1992

[54] Sudret B, Marelli S, Wiart J. Surrogate models for uncertainty quantification: an overview. Proceedings of the 11th European conference on antennas and propagation. 2017.

[55] Teixeira A, Rippi K, Schweckendiek T, Brinkman H, Nuttall J, Hellebrandt L, Courage W. Soil-structure interaction – Reliability analysis of a retaining wall, 2015. Delft, The Netherlands: Deltares & TNO; 2016.

[56] Timmermans ALJ. *Final design, combi-wall for inland barges, report number 101*. Project i.000770, offshore terminal sif. Rotterdam, The Netherlands: Port of Rotterdam Authority; 2017.

[57] ThyssenKrupp GfT Bautechnik. Spundwand-Handbuch berchnung. Gelsenkirchen, Germany: ThyssenKrupp GfT Bautechnik; 2007.

[58] Voogt H. Proactive and predictive waterfront asset management – Port of Rotterdam experience. Proceedings of the PIANC. 2014.

[59] Vrijling JK, Gelder PHAJMvan. The effect of inherent uncertainty in time and space on the reliability of flood protection. Saf Reliab 1998;1:451–6.

[60] Waarts PH. Structural Reliability Using Finite Element Analysis – an Appraisal of DARS: Directional Adaptive Response Sampling. Doctoral thesis Delft, The Netherlands: Delft University of Technology; 2000.

[61] Well TJvan der. Reliability-Based Assessment of Quay Walls MSc thesis Delft, The Netherlands: Delft University of Technology; 2018

[62] Wolters HJ, Bakker KJ, Gijt JGde. Reliability of quay walls using finite element analysis. Delft, The Netherlands: Delft University of Technology; 2012.